

Self-assembly of nanomaterials at fluid interfaces

Anju Toor^{1,3}, Tao Feng², and Thomas P. Russell^{2,3,a}

¹ Department of Mechanical Engineering, University of California, Berkeley, USA

² Department of Polymer Science and Engineering, University of Massachusetts, Amherst, USA

³ Materials Sciences Division, Lawrence Berkeley National Lab, Berkeley, USA

Received 29 February 2016 and Received in final form 23 April 2016

Published online: 31 May 2016 – © EDP Sciences / Società Italiana di Fisica / Springer-Verlag 2016

Abstract. Recent developments in the field of the self-assembly of nanoscale materials such as nanoparticles, nanorods and nanosheets at liquid/liquid interfaces are reviewed. Self-assembly behavior of both biological and synthetic particles is discussed. For biological nanoparticles, the nanoparticle assembly at fluid interfaces provides a simple route for directing nanoparticles into 2D or 3D constructs with hierarchical ordering. The interfacial assembly of single-walled carbon nanotubes (SWCNTs) at liquid interfaces would play a key role in applications such as nanotube fractionation, flexible electronic thin-film fabrication and synthesis of porous SWCNT/polymer composites foams. Liquids can be structured by the jamming of nanoparticle surfactants at fluid interfaces. By controlling the interfacial packing of nanoparticle surfactants using external triggers, a new class of materials can be generated that combines the desirable characteristics of fluids such as rapid transport of energy carriers with the structural stability of a solid.

1 Introduction

Liquid/liquid interfaces provide a versatile platform to generate advanced materials and structures. The assembly of nanomaterials with various geometries including nanoparticles (NPs), nanorods (NRs) and nanosheets at oil/water interfaces have advanced applications in polymer-based photovoltaic devices, magnetic data storage media, polymer composites, oil and mineral refining, coatings, detergents and pharmaceuticals. The driving force of an efficient assembly is the reduction of the interfacial energy between two fluids by the self-assembly of a layer of nanoparticles at the interface that act as a barrier between the fluids. These assemblies can be a spontaneous segregation of NPs to the interface or by the interfacial interactions of functionalized NPs dispersed in one fluid with ligands having complementary functionality dissolved in the second fluid, effectively converting the NPs into “nanoparticle surfactants”. The theory of an active assembly process, first developed by Pieranski to describe “Pickering emulsions”, is also applicable to NPs [1].

As shown in fig. 1, the placement of a single particle with an effective radius r , at the interface between water and oil phase leads to a decrease of the initial interfacial energy E_o (energy arising from the interface between the

liquids) to E_1 (energy with particles located at the interface), yielding an energy difference of ΔE_1 :

$$E_o - E_1 = \Delta E_1 = -\frac{\pi r^2}{\gamma_{O/W}} [\gamma_{O/W} - (\gamma_{P/W} - \gamma_{P/O})]^2.$$

Unlike colloidal particles, since the size of the NPs or r is small, ΔE_1 is small and thermal energy can be comparable to ΔE_1 , resulting in adsorption and desorption of the NPs at the interface, *i.e.* the assemblies are dynamic, and in the plane of the interface the packing of the NPs is liquid-like in nature. By the formation of NP-surfactants at an interface, however, ΔE_1 per particle is increased significantly, since the NP-surfactants are essentially multiple surfactants wrapped into one species. Remarkably, the number of ligands associating with the NPs is self-regulating whereby the reduction in the interfacial energy per NP is maximized. This alleviates having to precisely modify the surface functionality of the NPs to maximize the reduction in the interfacial energy per NP. By controlling the strength of interactions between the ligands and the NPs, one has a versatile tool by which the assemblies of the NP-surfactants can be made responsive to external stimuli. Since the assemblies are at liquid interfaces, the NPs and ligands are easily accessed by reactants added to either liquid phase, so the strength of association between the NPs and ligands can be manipulated or the functionality of the NPs and ligands can be altered. A simple case

^a e-mail: russell@mail.pse.umass.edu

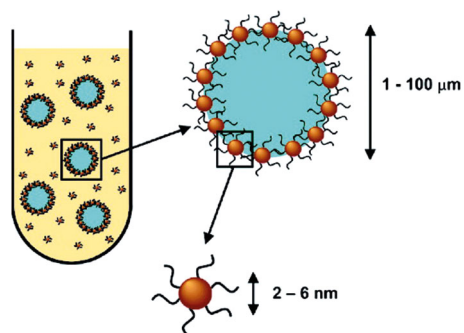


Fig. 1. Schematic of self-assembly of nanoparticles at a fluid-fluid interface. Reprinted with permission from *Langmuir* [2] © (2005) American Chemical Society.

in point would be where the NPs and ligands are interacting by hydrogen bonding and, by altering the pH, the strength of the bonding can be changed. This becomes particularly important when a lateral force is placed on the NP-surfactant assemblies that compresses the assemblies, possibly forcing a desorption of the NP-surfactants from the interfaces, as seen with simple NPs. The extent of interactions and anchoring of the ligands to the NP, NR and nanosheet surfaces can be used to control functionality, wettability and the magnitude of the energy change holding them at the interface, which makes these NP-surfactants quite versatile. In this contribution, the recent advances of the assembly of NPs, NP-surfactants, NRs and nanosheets at the oil/water interfaces will be thoroughly reviewed. We will rely heavily on examples that are taken from research in our laboratories, though this has been a very active area of research in numerous laboratories worldwide, and comprehensively covering this entire field in this review is not possible.

2 Interfacial assembly of nanomaterials

2.1 Homogeneous nanoparticle assembly at fluid interfaces

Reincke *et al.* [3] observed that non-functionalized, charged gold nanocrystals can spontaneously assemble, forming a monolayer at the water/oil interface on gradually reducing the surface charge of the nanocrystals. Charge stabilized gold nanocrystals with diameters between 8 and 40 nm were prepared. The as-prepared gold nanocrystals have negative charge due to the adsorption of citrate and gold chloride anions. Figure 2(a) (left) shows a vial containing the aqueous gold solution with an immiscible layer of heptane on top. Upon addition of ethanol to this solution, a blue layer is spontaneously formed at the water/oil interface, as shown in fig. 2(a) (centre and right). The addition of ethanol gradually reduces the surface charge on the gold nanocrystals; the nanocrystal coverage of the water/oil interface increases with decrease in the surface charge. Figure 2(b) is a transmission electron microscopy (TEM) image of the nanocrystal layer collected from the heptane/water interface. It shows that



Fig. 2. (a) Left: an aqueous gold solution (pink) covered with heptane (colorless); centre and right: after the addition of 4 mL ethanol to the solution, a gold nanocrystal layer (blue) is formed at the heptane-water interface and extends up the heptane-glass interface. Gold nanocrystals are extracted from the water phase, but do not transfer to the heptane phase. (b) TEM image of a layer with maximum coverage (65%) collected from the heptane-water interface shows that the layer does not contain 3D aggregates; the voids have a typical size equivalent to 1–10 nanocrystals; the space between particles is 1–4 nm. Reprinted with permission from *Angew. Chem. Int. Ed.* [3] © (2004) Wiley-VCH.

the layer is not ordered, the layer has voids with size equivalent to 1–10 nanocrystals and the interparticle spacing is 1–4 nm.

Wu and coworkers have developed this self-assembly technique into a novel and facile strategy to fabricate nanofilm-based devices such as photodetectors [4–9]. Hu *et al.* [4] successfully fabricated the NiCo_2O_4 nanofilm by the interfacial assembly of NiCo_2O_4 platelets. NiCo_2O_4 is a promising material for photodetectors due to its proper bandgap of ≈ 2.1 eV [10]. A typical NiCo_2O_4 platelet crystallite exhibits a uniform hexagonal shape with sharp corners. These highly crystallized platelets were self-assembled at a hexane/water interface using ethanol as an inducer. The monolayer of high quality formed at the interface was transferred onto a solid substrate by lifting-up approach (fig. 3(a)). In order to minimize any free space at the interspace in the monolayer film, this deposition process was repeated twice to obtain a two-layer NiCo_2O_4 film. Figure 3(b) shows the SEM image of the two layer NiCo_2O_4 film, which confirms that NiCo_2O_4 platelets were aligned parallel to the substrate to form a densely packed film. The photodetector device constructed from this NiCo_2O_4 platelet film showed good sensitivity, excellent stability, and fast response time, justifying the effective utilization of this type of film device as promising high-frequency photodetectors.

Chen *et al.* [9] extended this oil-water interfacial assembly to fabricate ZnO hollow-sphere nanofilms. The PS-ZnO core-shell nanospheres were dispersed at a hexane-water interface to form a densely packed film. The assembled film was transferred onto a silicon substrate with a 200 nm SiO_2 top layer, followed by annealing at 600 °C for 3 h in air to obtain a ZnO hollow-sphere nanofilm. TEM and high-resolution TEM (HRTEM) images for the ZnO hollow spheres are shown in fig. 4(a) and (b) respectively. It is evident that the shell of each hollow sphere is composed of numerous ZnO nanocrystals with size of ≈ 10 –20 nm. Figure 4(c) shows the scanning electron microscopy (SEM) image of the ZnO hollow-sphere

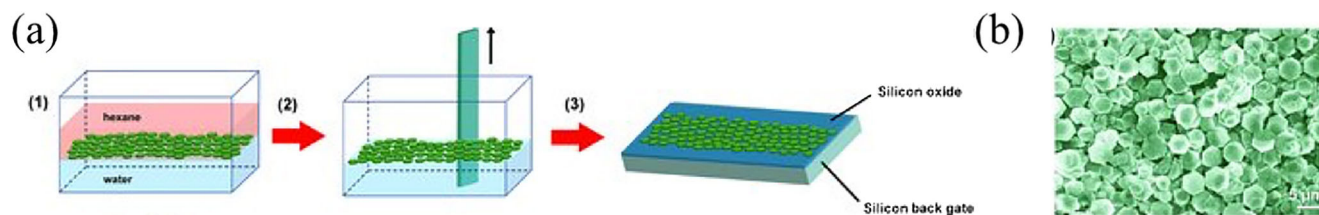


Fig. 3. (a) Schematic illustration of the fabrication procedure of NiCo_2O_4 nanofilm through an interfacial assembly strategy. 1) Self-assembly of NiCo_2O_4 platelets at the hexane/water interface into a monolayer film, 2) removal of the hexane phase using a syringe, 3) transfer of the as-assembled film to a SiO_2/Si substrate. (b) Typical SEM image of the NiCo_2O_4 two-layer film. Reprinted with permission from *Adv. Mater.* [4] © (2011) Wiley-VCH.

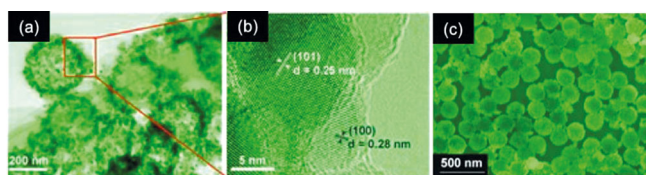


Fig. 4. Typical (a) TEM and (b) HRTEM images of the ZnO hollow spheres. (c) SEM image of the ZnO hollow sphere nanofilm deposited on a SiO_2/Si substrate. Reprinted with permission from *Small* [9] © (2011) Wiley-VCH.

nanofilm. The substrate is densely covered by a large number of ZnO hollow spheres with average diameter of about 260 nm.

Lin *et al.* [2] investigated the assembly of Tri-n-octylphosphineoxide (TOPO) covered CdSe nanoparticles at toluene/water interfaces. Figure 5A shows a fluorescence confocal microscopy image of water droplets dispersed in toluene where the CdSe nanoparticles are assembled at the interface. Figure 5B shows an optical microscopy image of nanoparticle stabilized water droplets that were dried on a silicon substrate. Using scanning force microscopy (SFM), the thickness of the nanoparticle assembly was measured to be 15 ± 3 nm, roughly twice the diameter of the TOPO-covered CdSe nanoparticles. This implies that a monolayer of nanoparticles assembled at the fluid interface. Figure 5(C) shows an electron microscope image of the water droplets collected on a TEM grid. The autocorrelation function of the TEM image is shown in the inset. The mean interparticle spacing of 7.2 nm is comparable to the effective diameter of the ligand functionalized CdSe nanoparticles. These results suggest that nanoparticles segregated to the fluid interface and the particle assembly exhibits a liquid-like packing.

By cross-linking the nanoparticles adsorbed at the interface, mechanically robust membranes and capsules can be fabricated from the spherical nanoparticle assemblies. Lin *et al.* [11] utilized the chemical cross-linking of the ligands attached to the CdSe nanoparticles for obtaining robust nanoparticle assemblies. A toluene dispersion of CdSe nanoparticles of diameter 2.9 ± 0.2 nm and functionalized with reactive vinylbenzene moieties was added to an aqueous solution of 2,2'-azobis(2-(2-imidazolin-2-yl)propane) dihydrochloride to obtain an assembly of nanoparticles.

CdSe nanoparticles assembled at the water/oil interface and formed a membrane of cross-linked particles upon

heating in a controlled atmosphere. These membranes maintained their integrity even after the removal from the fluid interface (fig. 6). This implies that nanoparticles can be used as building blocks for nanoporous membranes and capsules. A disadvantage of the crosslinking technique is the elevated temperature required for initiating the cross-linking of the vinyl benzene ligands. But, ligands systems that allow cross-linking at room temperature have now been developed.

2.2 Nanorods/nanotubes assembly at fluid interfaces

Recent advances in the synthesis of inorganic nanoparticles have provided nanoscopic objects that are anisotropic in shape. Nanorods, for example, have attracted great interest for the fabrication of functional materials with novel optical, electrical, and magnetic properties. The interfacial activity of nanorods can be explained by the reduction of interfacial energy. The concentration of nanorods in solution limits the total number of nanorods that can assemble at the interface, which is determined by the chemical potential difference of the nanorods at the interface and in the bulk solution. For nanorods oriented parallel or perpendicular to the fluid interface, the energy change for placing the nanorods at the interface is given by [12]

$$\Delta E_{\parallel} = 2\pi RL[\pi(\gamma_{P/O} - \gamma_{P/W}) + \theta(\gamma_{P/W} - \gamma_{P/O}) + \gamma_{O/W} \sin \theta],$$

where

$$\cos(\theta) = \frac{(\gamma_{P/W} - \gamma_{P/O})}{\gamma_{O/W}} \quad (L \gg R),$$

$$\Delta E_{\perp} = (\gamma_{P/W} - \gamma_{O/W} - \gamma_{P/O})\pi R^2 + (\gamma_{P/W} - \gamma_{P/O})2\pi Rh.$$

The energy change associated with nanorods assembly when the nanorods are oriented parallel to the interface is defined as ΔE_{\parallel} , and ΔE_{\perp} is the energy change when the nanorods are oriented perpendicular to the interface. R is the effective radius, L is the length of the rods, and γ denotes the interfacial energy, P , O , W and θ represent the particle, oil, water and the contact angle of the particle at the interface, respectively. The penetration depth of the nanorods into the water phase, when assembled normal to the interface, is defined as h . These

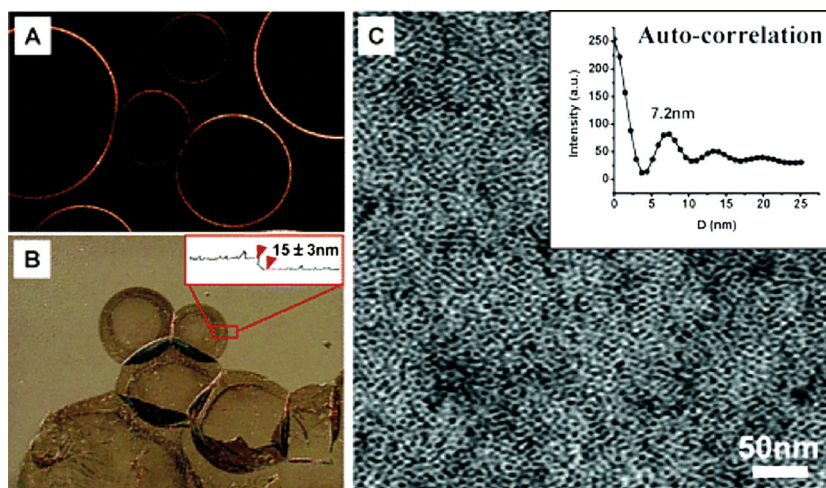


Fig. 5. (A) Fluorescence confocal microscopy image of CdSe nanoparticles covered water droplets dispersed in toluene. (B) Differential interference contrast optical microscopy image of dried droplets on a silicon substrate. Inset: AFM height section analysis. (C) TEM image of a dried droplet. Inset: Autocorrelation function of the TEM image. Reprinted with permission from *Langmuir* [2] © (2005) American Chemical Society.

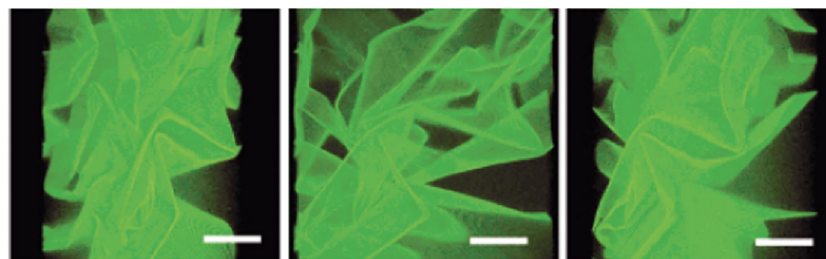


Fig. 6. Confocal microscopy image of a nanoparticle sheet prepared by cross-linking the vinyl benzene ligands. The scale bar is 50 μm . Reprinted with permission from *J. Am. Chem. Soc.* [11] © (2003) American Chemical Society.

expressions predict that isolated nanorods orient parallel to the plane of the interface so as to maximize the interfacial coverage per particle and minimize the Helmholtz free energy of the system (fig. 7). With increasing nanorod concentration in the bulk solution, the interfacial tension decreases until the fluid interface is saturated with randomly packed nanorods oriented parallel to the interface. Upon further increase in concentration, separation distance between nanorods decreases to a critical point at which nanorods are forced to reorient normal to the interface to further reduce the energy of the system [12, 13].

He *et al.* [12] studied the self-assembly of Tri-*n*-octyl-phosphine oxide (TOPO) covered cadmium selenide (CdSe) nanorods at an oil-water interface. Water droplets were obtained by adding water (10% volume fraction of the oil phase) into a dispersion of the TOPO-covered CdSe nanorods in toluene, followed by vigorous shaking. CdSe nanorods dispersed in toluene initially, assembled at the water/toluene interface, and stabilized the dispersion of water droplets forming Pickering emulsions. The TOPO-covered droplets in toluene were rinsed with pure toluene and the toluene was allowed to evaporate, leaving nanorods embedded on a water droplet in contact with air. The TEM image of a droplet is shown in fig. 8. The assembly of nanorods exhibit a range of two-dimensional structures with different orientations. The structures ob-

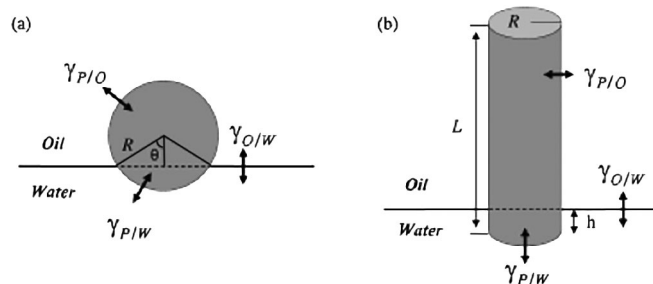


Fig. 7. Schematic image of nanorods oriented parallel (a) and perpendicular (b) to the oil/water interface. R is the effective radius of the rods, L the effective length of the rods and γ the interfacial energy. P , O , W , and θ represent the particle, oil, water, and the contact angle of the particle at the interface, respectively; h is the depth of nanorods in the water phase when placed vertical to the interface. Reprinted with permission from *Small* [12] © (2007) John Wiley and Sons.

served span the range of the phase diagram, from a low-density smectic packing to a more dense columnar ordering to a crystalline-like phase. By controlling the interfacial energy between different liquids and nanoparticles, the aspect ratio of the nanorods, and their concentration, the lateral packing of the nanorods can be varied. Such control over self-assembly is key in designing hierarchi-

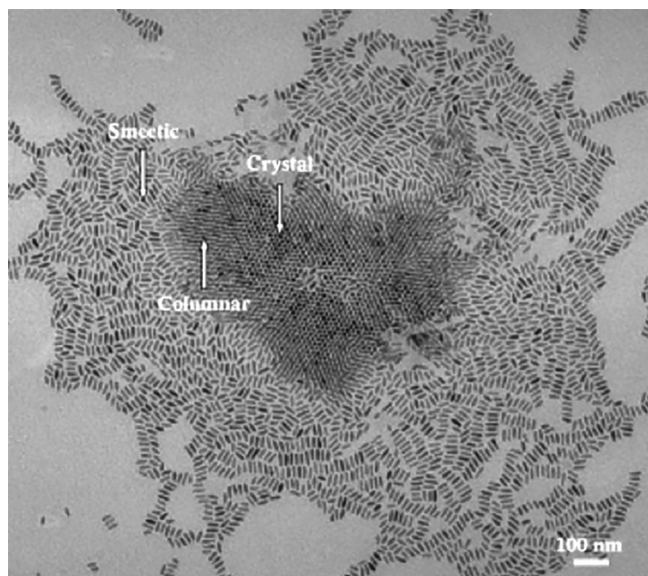


Fig. 8. TEM image of a TOPO-covered CdSe-nanorod-stabilized water droplet after drying on a carbon-coated copper grid. Reprinted with permission from *Small* [12] © (2007) John Wiley and Sons.

cally ordered structures that will open new opportunities in fabricating optical, acoustic, electronic, and magnetic materials and devices.

3 Biological nanoparticles

Biological nanoparticles offer unique advantages, in particular truly monodisperse particles and the availability of a wide range of surface functionalities for modification on the protein shell. Self-assembled bionanoparticles have been used in last few years as building blocks and templates in bionanotechnology [14, 15]. Bionanoparticles such as cowpea mosaic virus (CPMV), tobacco mosaic virus (TMV), turnip yellow mosaic virus (TYMV), M13 bacteriophage and ferritin have been used in the field of self-assembly. Self-assembly of biological nanoparticles at a fluid-fluid interface can provide a simple and fast route for the assembly of bionanoparticles into 2D or 3D constructs with hierarchical ordering. Here, we will review cowpea mosaic virus, tobacco mosaic virus, and ferritin bionanoparticles.

Cowpea mosaic virus is a plant virus that measures approximately 30 nm in diameter and exhibits an icosahedral symmetry. The structure is well characterized to atomic resolution, and the viral particles are thermostable upto 65 °C. CPMV capsids are stable in some organic solvents, up to 20% DMSO or dioxane that is an important requisite for effecting crosslinking reactions at interfaces. CPMV is a particularly attractive biological nanoparticle because its surface chemistry has been extensively studied. By modifying the virus surface, novel properties can be imparted enabling nanotechnological applications in biosensors, catalysis and nanoelectronic devices. Biological nanoparticles can be used for forming Pickering

emulsions. CPMV can be assembled at the perfluorodecalin/water interface and cross-linked using glutaraldehyde in the water phase [16]. Pickering emulsions having 10–100 μm diameter droplets were obtained on sonicating a mixture of perfluorodecalin and dispersion of fluorescently labeled CPMV in buffer solution.

Figure 9(a) shows 3D reconstructed perfluorodecalin droplets coated with CPMV after cross-linking and removal of excess CPMV particles in the buffer phase by fluorescence confocal microscopy. The complete removal of water and perfluorodecalin disrupts the crosslinked CPMV shell around the oil phase, with the resulting crumpled morphology after rehydration displayed in fig. 9(b). The crosslinked nanoparticle films, when placed on a glass slide, leads to the formation of a spherical cap (fig. 9(c)), from which the thickness is determined by SFM. The cross-sectional analysis from a uniform area, specified in the white box in fig. 9(d), gives a step height of 29.2 nm, which is consistent with that of a monolayer formed by virus particles of 28–32 nm in diameter.

Tobacco mosaic virus (TMV) has a rigid hollow cylinder structure that measures approximately 300 nm in length and 18 nm in diameter. It has ~ 2130 protein subunits arranged helically around single stranded RNA, forming an internal channel of 4 nm diameter. The surface properties of TMV can be easily modified chemically or genetically without altering the structure and integrity of TMV particles. The protein shell of TMV provides a robust tube-like scaffold for the preparation of nanoscale materials. Tobacco mosaic virus bionanoparticles can assume different orientations when assembled at oil-water interface [17]. Depending on the initial concentration of TMV, these bionanorods can assume different orientations. He *et al.* [17] observed that TMV orients parallel to the interface at low concentrations, whereas at higher concentrations, TMV nanorods are oriented normal to the interface.

Likewise, ferritin nanoparticles can also be used as Pickering emulsifier forming a closed-packed array on droplet surface [18]. Ferritins are composed of 24 subunits arranged in octahedral symmetry, which self-assemble into form a 12 nm diameter cage with a 7.58 nm diameter cavity, known as Apoferritin. Ferritin nanoparticles are able to co-assemble with ligand functionalized inorganic particles such as CdSe at the oil-water interface [19].

The cross-linked co-assemblies of the benzaldehyde covered CdSe nanorods with ferritin particles at a planar chloroform-water interface was imaged by TEM (shown in fig. 10), clearly showing the coexistence of both ferritin particles (blue circles) and CdSe nanorods (red ovals).

4 Cooperative interfacial assembly of nanoparticles

4.1 Interfacial assembly of acid-treated SWCNTs

Recently, the extraordinary properties of carbon nanotubes (CNTs) have motivated significant interest in application areas as diverse as biosensors, capacitors, battery electrodes, catalysts, actuators, transistors, and mem-

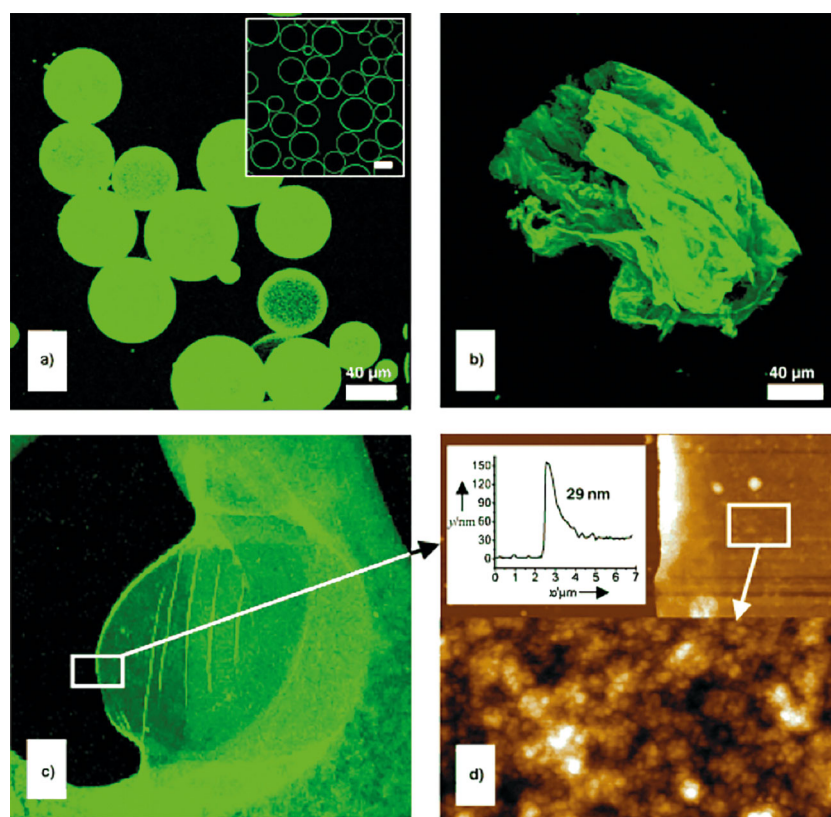


Fig. 9. Confocal fluorescence microscopy image of CPMV particle assembly after cross-linking with glutaraldehyde. a) 3D reconstruction of the virus coated perfluorodecalin droplets in water (inset: cross-sectional view). Excess particles were removed by successive washing with water. b) Crumpled droplet after complete drying and rehydration with water. c) Capsule cap after complete drying. d) The white box shows the area at which the SFM scan was taken, and the lower part shows the height profile on top of the collapsed capsule (image width = $2\ \mu\text{m}$, z range = $30\ \text{nm}$). Reprinted with permission from *Angew. Chem. Int. Ed.* [21] © (2005) John Wiley and Sons.

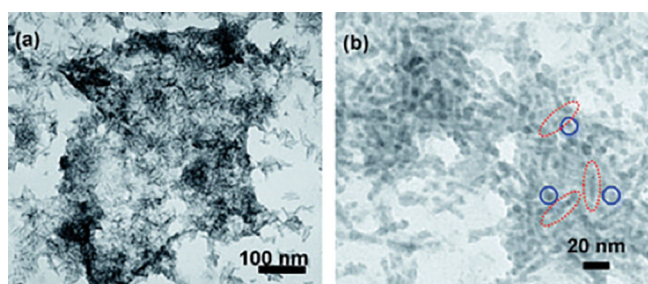


Fig. 10. TEM images of a cross-linked sheet made by co-assembly of ferritin and CdSe nanorods at a chloroform-water interface (a) low magnification image, and (b) high magnification image showing individual CdSe nanorods (red ovals) and ferritin particles (blue circles). Reprinted with permission from *Soft Matter* [17] © (2009) Royal Society of Chemistry.

branes, many of which can be established upon the platform of liquid-liquid interfaces. The interfacial segregation of single-walled carbon nanotubes (SWCNTs) between two immiscible liquid phases is one of key steps towards numerous applications like nanotube fractionation, flexible electronic thin-film fabrication, the synthesis of porous SWCNT-polymer composites foams. Nonethe-

less, relatively little is known about CNT behavior at liquid-liquid interfaces. One of the early pioneering studies was done by Wang where pristine, amphiphobic SWCNTs can act as natural “surfactants” to stabilize macroscopic Pickering emulsions comprised of water droplets in toluene [20]. They further improved the solubility and interfacial activity of SWCNTs by introducing surfactants, deoxycholate (DOC) [21] or ss-DNA [22] and prepared microscopic polymer colloids coated with length- and type-sorted SWCNTs.

Feng *et al.* developed an easy and efficient, two-step method to segregate SWCNTs at the toluene/water interface [23]. The first step includes an acid mixture treatment accompanied by sonication to achieve an aqueous dispersion and a shortening of the CNTs. In the oxidation procedure, it was confirmed by infrared and Raman spectroscopy that defects in SWCNT graphitic structure are oxidized into phenol, quinone, carboxylic acid, and other oxidized carbon functionalities, the “damage” sites irregularly accumulated along the tube length.

With the graphitic network increasingly disrupted, accompanying sonication causes a near statistical shortening of SWCNT length as oxidation proceeds. Most of the cut lengths fell across the span 50–300 nm confirmed

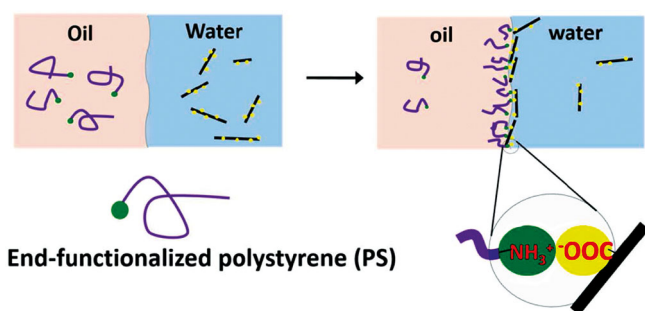


Fig. 11. Cooperative interfacial segregation between acid-treated SWCNTs and PS-NH₂.

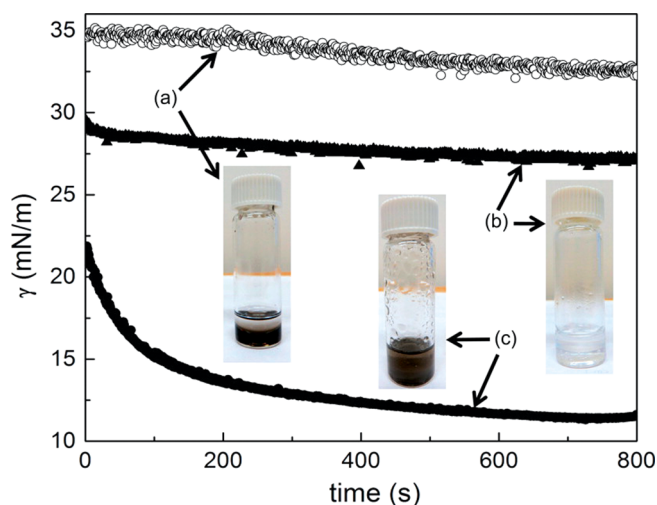


Fig. 12. Time dependence of surface tension γ . (a) Top layer: toluene; bottom layer: acid-treated SWCNT aqueous dispersion. (b) Top layer: PS-NH₂ in toluene; bottom layer: water. (c) Top layer: PS-NH₂ in toluene; bottom layer: acid-treated SWCNT aqueous dispersion. Inset images show that emulsification was achieved only in sample c ($C_{\text{PS-NH}_2} = 0.2$ mg/ml, $C_{\text{SWCNT}} = 0.08$ mg/ml, PS-NH₂ $M_n = 2,800$ g/mol, 6 h SWCNT acid treatment). Reprinted with permission from *Langmuir* [23] © (2014) American Chemical Society.

by dynamic light scattering. These acid treated SWCNTs can be easily and stably dispersed in water; no evidence of aggregation in pure water was noted after several months of storage. Subsequently, a hydrophobic component, amine-terminated polystyrene (PS-NH₂) was introduced into toluene phase, which was shown in fig. 11. The strong electrostatic coupling between protonated terminal amine at polystyrene chain end and carboxyls on nanotube surfaces drives SWCNTs segregation and assembly towards toluene/water interfaces.

The assembly of SWCNT cooperatively with PS-NH₂ was probed by pendant drop tensiometry.

Figure 12 shows that with the presence of two cooperative components, *i.e.*, SWCNT in aqueous and PS-NH₂ in toluene, the interfacial tension undergoes a massive reduction with its steady-state value comparable to that of a conventional small surfactant.

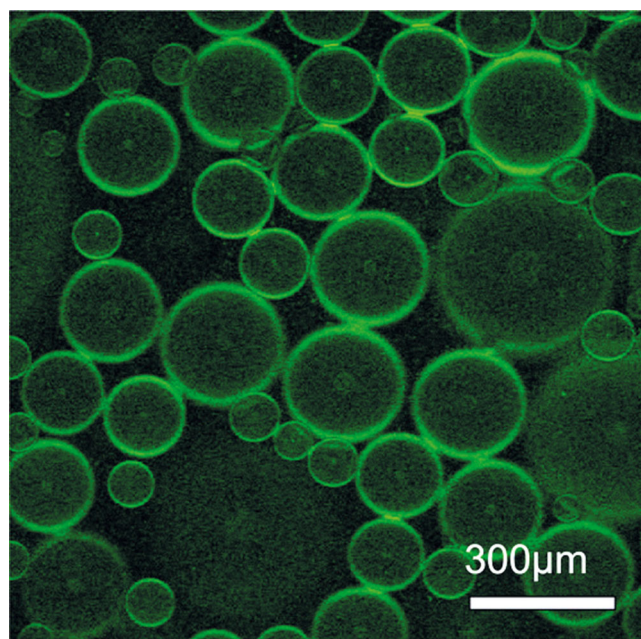


Fig. 13. Confocal fluorescence micrograph of water-in-toluene emulsion droplets stabilized by the cooperative interfacial segregation of acid-treated SWCNTs and PS-NH₂. The SWCNTs are fluorescently labeled. ($C_{\text{PS-NH}_2} = 0.1$ mg/ml, $C_{\text{SWCNT}} = 0.08$ mg/ml, PS-NH₂ $M_n = 2,800$). Reprinted with permission from *Langmuir* [23] © (2014) American Chemical Society.

The significant surface tension lowering indicates a strong segregation for the complex of SWCNT/PS-NH₂. Alongside with surface tension change, it was found that this SWCNT/PS-NH₂ “nanosurfactant” is capable of generating highly stabilized water-in-oil emulsions. Figure 13 shows LSCFM images of 100–300 μm aqueous phase emulsion droplets, and the fluorescence localization consistent with strong interfacial SWCNT segregation is evident.

The physical chemistry study of Feng *et al.* suggests an easy manipulation in comparison to a direct delicate functionalization of SWCNT surfaces. An effective tuning of segregation capability can be achieved either by varying the polymer chemistries or the physicochemical conditions of the liquid phases. As far as materials chemistry is concerned, it was revealed that the end functionality and the molecular weight of PS, have significant impact on the segregation (fig. 14). A strong segregation occurs only with quarternizable amine chain-end, a necessary condition for electrostatic interaction to take effect. Likewise, as PS-NH₂ M_w grows ($\gtrsim 10,000$ g/mol), segregation is severely attenuated due to the large entropic penalty caused by interfacial chain adsorption. On the other hand, upon changing the physical condition of liquid phase, shown in fig. 15 by the interfacial tension change, pH was found to enable a unique, sharp transition of SWCNT segregation at the solution pH equal to the pK_a of carboxylic acid group, a major functionality on SWCNT surface. Shown in fig. 16, at pH above the pK_a of carboxyl groups, the SWCNT carboxyl groups are mostly ionized. The high charge density along the tubes gives rise to strong repulsion, higher than

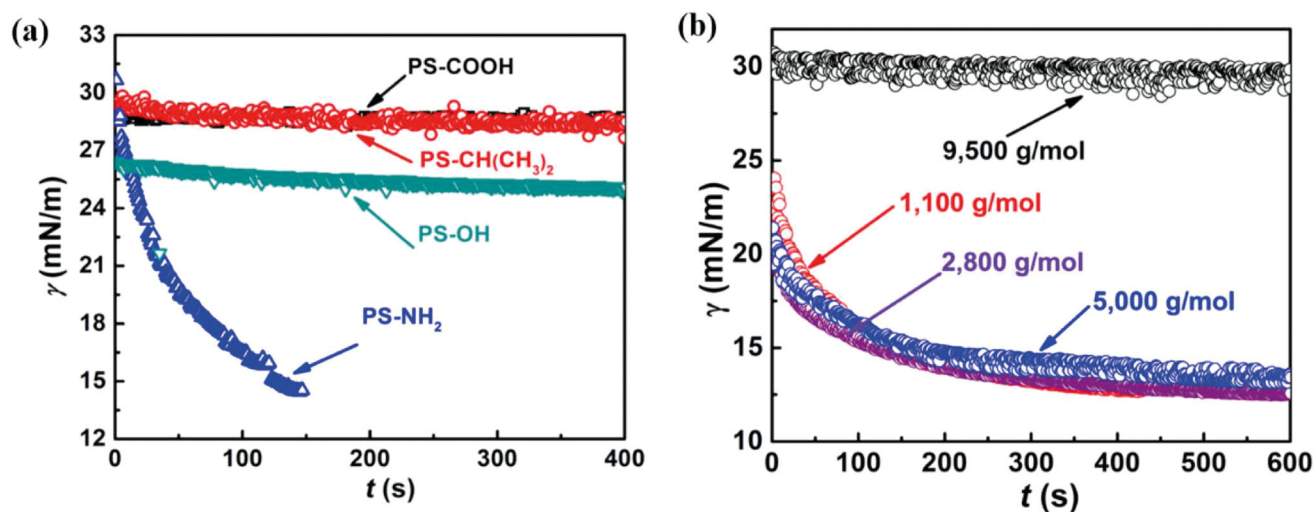


Fig. 14. (a) Impact of PS end-group chemistry on the time evolution of interfacial tension γ (PS $M_n \sim 2,000$ g/mol, $C_{PS} = 0.5$ mg/ml, $C_{SWCNT} = 0.08$ mg/ml, $pH \sim 3.5$, 6 h SWCNT acid treatment). (b) Impact of PS-NH₂ molecular weight on the time evolution of interfacial tension γ (PS-NH₂ $M_n \sim 2,800$ g/mol, $C_{PS} = 0.5$ mg/ml, $C_{SWCNT} = 0.08$ mg/ml, $pH \sim 3.5$, 6 h treated SWCNTs).

the association energy, between SWCNTs that inhibits an efficient segregation at liquid/liquid interfaces. Whereas below the pK_a , where the carboxyl groups are mostly non-ionized, this repulsion is markedly suppressed and a strong segregation can occur with only reduced surface charge. Apart from charge density regulation induced by pH , another character of acid-treated SWCNTs, termed multivalency (*i.e.* multiple functionalization) also contributes to the observed transition behavior. This cooperative assembly technique and the physical chemistry can be easily extended to other materials bearing similar functionality, which imparts valuable guidance for manipulating nano-materials assembly at liquid/liquid interfaces.

4.2 Interfacial assembly of graphene oxide sheets (GO)

In contrast to carbon nanotubes and nanoparticles, graphene oxide is an atomically thin sheet with a hydrophobic basal plane and the hydrophilic functionalities at its peripheral. The interfacial assembly of GO sheets at liquid/liquid interfaces opens a new route to fabricate graphene films for electronic or thin-film applications. The planar, flexible geometry allows this nanosheet to conform to a curved interface, making it as an effective barrier to stabilize one liquid in another. It was found that the GO only possesses limited segregation capability at the oil/water interfaces. The attenuated amphiphilicity can arise from the improper ratio of hydrophilic functionality on the edge to the area of hydrophobic graphitic plane, making it less likely to dwell at the interface.

To enhance the surfactancy of hydrophilic GO, Sun *et al.* developed a simple route by adding a block copolymer ligand, polystyrene-*b*-poly (vinyl pyridine) (PS-*b*-PVP), that interacts favorably with the hydrophilic GO (fig. 17). It was found that the GO can be effectively trapped at

the toluene/water interfaces and jammed into solid thin films via electrostatic or hydrogen bonding interaction with quaternized pyridine unit. Figure 18(a) shows the dynamic interfacial tension as different concentrations of GO are introduced into the aqueous phase. A remarkable interfacial energy reduction was noted in the presence of polymer with the equilibrium value increases with the concentration of GO. As the GO concentration increases, the nanosheets prevent a substantial assembly of polymer chains by occupying large interfacial area with its basal plane, giving rise to higher saturation value of interfacial tension. The buckling of interface upon compression indicates the formation of an elastic thin film (fig. 18(b)). The assembled, robust interfacial GO films, showing tessellated morphology in TEM micrographs (fig. 19), can withstand large shrinkage and remain intact even when the droplet was completely withdrawn back into the needle.

The assembly kinetic studies show the GO adsorption as the rate-controlling step and the surface coverage can be up to 90%, nearly encompassing entire interface. This liquid/liquid interfacial assembly provide a facile way to prepare large area graphene films as well as stabilize liquid phase.

4.3 Nanoparticle surfactants

Nanoparticles assembly at fluid interfaces can be utilized to form surfactants. Recently, Cui *et al.* [25] found that using amine-terminated polydimethylsiloxane in oil and carboxylic acid functionalized nanoparticles dispersed in water, nanoparticle surfactants can be formed *in situ* due to the carboxylate-amine electrostatic interactions. It was observed that stable non-equilibrium liquid shapes can be generated utilizing the nanoparticle surfactants. In addition, these shapes can be easily controlled using an electric

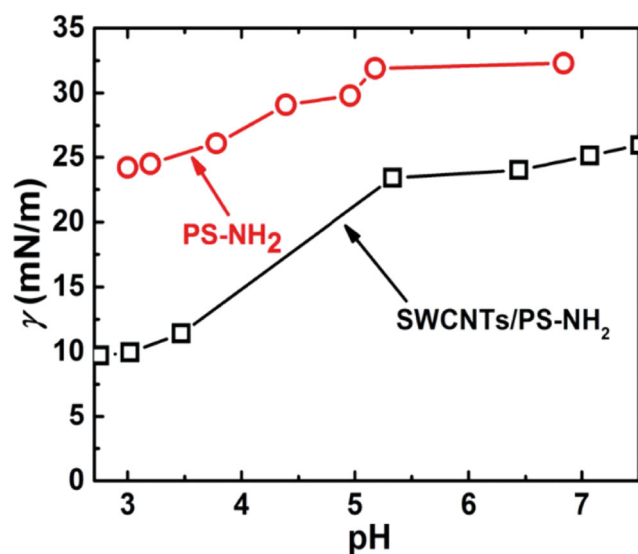


Fig. 15. Steady-state γ as a function of SWCNT solution pH (red: without SWCNTs in aqueous phase; black: with SWCNT in aqueous phase, $C_{\text{SWCNT}} = 0.5 \text{ mg/ml}$, initial $pH \sim 2.7$).

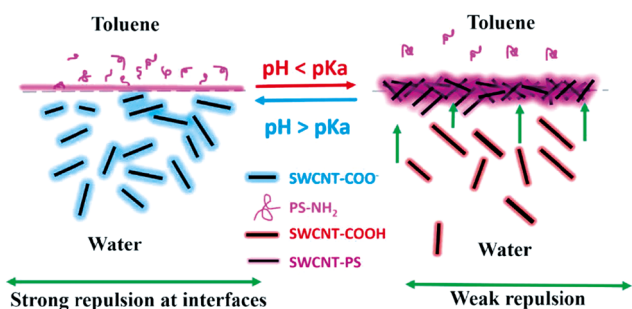


Fig. 16. Physical depiction of pH -induced, SWCNT segregation transition at the toluene/water interfaces (2003) American Chemical Society.

field (fig. 20). For these experiments, a droplet of aqueous phase containing nanoparticles was first created in an oil phase comprising of a mixture of silicone oils, with an amine-terminated polydimethylsiloxane (PDMS) followed by the application of the electric field. It was observed that shape of droplet gets distorted from spherical to ellipsoidal giving rise to an increased interfacial area for the same droplet volume. Hence, allowing more nanoparticle surfactants to form and assemble at the water/oil interface.

Figure 21(A) shows the deformation of the spherical water drop under the applied electric field of 4.6 kV/cm , increasing the surface area from 40.7 to 193.2 mm^2 . With time, the deformed droplet stretches further, increasing the major axis of the ellipsoid, while the minor axis decreases, to a certain extent where the increase in interfacial energy balances the applied electric field force. Upon removal of the electric field, the deformation of the drop decreases, reducing the surface area to 189.0 mm^2 , where the nanoparticle surfactants are jammed at the interface.

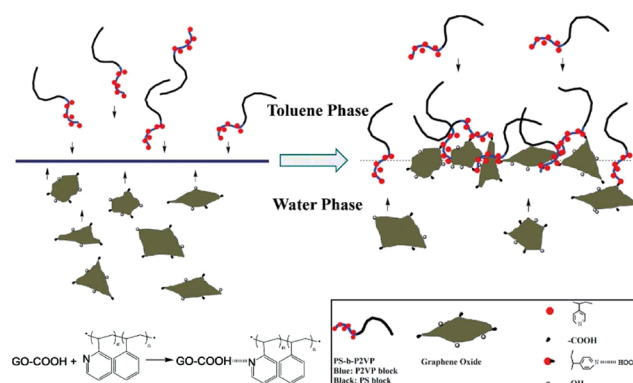


Fig. 17. Assembly of graphene oxide and block copolymer at the toluene/water interface. Reprinted with permission from *Langmuir* [24] © (2013) American Chemical Society.

It can be seen from fig. 21(B) that the deformed water droplet remained stable even after one month.

The deformation of the water drop containing polystyrene nanoparticles in a silicone oil containing amine-terminated PDMS is shown in fig. 21(C). It reaches an asymptotic value dictated by the strength of the electric field and the number of nanoparticle surfactants formed at the water-oil interface. In fig. 21(D), when only nanoparticles are dispersed in the water phase, the drop deformation is identical to that seen with pure water in oil. With only amine-terminated PDMS in the oil phase, the rate at which deformation (D) changed with E^2 was 2.1 times higher than the nanoparticles only case. This implies that the functionalized PDMS acts like a surfactant. However, the drop returned to its spherical shape upon the removal of electric field. With the nanoparticles and end functionalized PDMS in the water and oil phases, respectively, the rate at which D increased with E^2 was 2.6 times higher than the pure fluids, indicating a further reduction in interfacial tension due to the *in situ* formation of the nanoparticle surfactants.

As discussed previously, the formation of the nanoparticle surfactants is due to the electrostatic interactions between nanoparticles and the end functionalized polymer ligand therefore, the assembly of the NP-surfactants at the water/oil interface can be controlled by adjusting pH . Huang *et al.* [26] studied the effect of pH on electrostatic interactions for the water/silicone oil system. An aqueous droplet containing carboxylated polystyrene nanoparticles was suspended in a mixture of oils containing amine-terminated polydimethylsiloxane (PDMS-NH₂) followed by the application of an electric field (4.8 kV/cm) which deformed the droplet into an ellipsoidal shape. The relaxation of the droplet to its original shape upon removal of the electric field, was contingent on the pH of the aqueous phase. For higher pH (> 5), the droplet remained in the ellipsoidal shape owing to the strong interactions between the carboxylates and the protonated amine groups. Whereas at lower pH (4.3 – 5), the interactions become weak causing the removal of nanoparticle surfactants which resulted in the relaxation of the deformed droplet to its original spherical shape (fig. 22(a)).

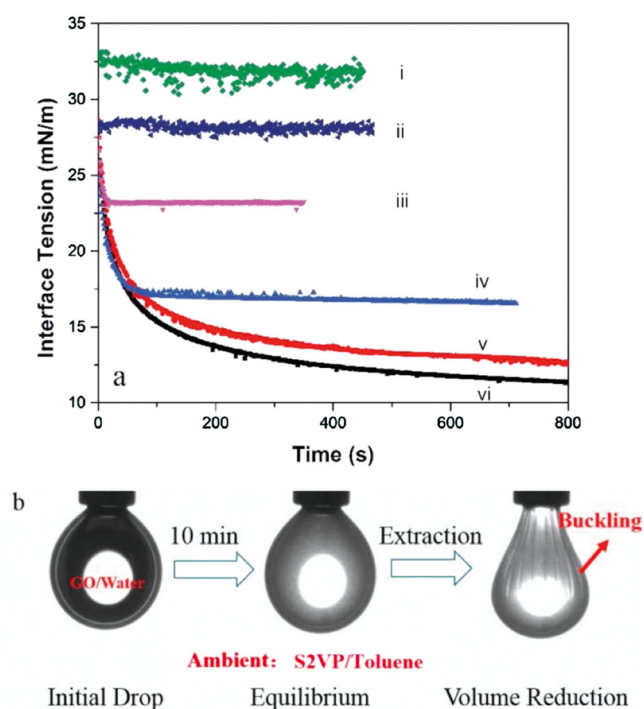


Fig. 18. (a) Dynamic interfacial tension of the toluene/water interface at different concentrations of graphene oxide and S2VP19.5k block copolymer: i) water against toluene, ii) $0.12 \text{ g} \cdot \text{L}^{-1}$ GO/water against toluene, iii) $0.25 \text{ g} \cdot \text{L}^{-1}$ GO/water against $0.10 \text{ g} \cdot \text{L}^{-1}$ S2VP19.5k/toluene, iv) $0.12 \text{ g} \cdot \text{L}^{-1}$ GO/water against $0.10 \text{ g} \cdot \text{L}^{-1}$ S2VP19.5k/toluene, v) $0.04 \text{ g} \cdot \text{L}^{-1}$ GO/water against $0.10 \text{ g} \cdot \text{L}^{-1}$ S2VP19.5k/toluene, and vi) water against $0.10 \text{ g} \cdot \text{L}^{-1}$ S2VP19.5k/toluene. (b) Buckling of the droplet surface assembled with graphene oxide, corresponding to line iv) Reprinted with permission from Langmuir [33] © (2013) American Chemical Society.

The weakening of the electrostatic interactions between nanoparticles and PDMS- NH_3^+ is due to the protonation of the carboxylate (pK_a of carboxylic acid group ~ 4.2) which effectively reduced the charge density on the surface of nanoparticle. A schematic of the assembly behavior between nanoparticles and polymer ligands at an oil/water interface is shown in fig. 22(b). The number of potential interactions between nanoparticles and polymer end groups reduces with decrease in pH below 5.

This dependence of the NP-surfactant interfacial activity on pH suggests that pH can be used as a means of triggering changes to NP-surfactant assemblies and the jammed state of the assemblies. The adjustment of pH, can be affected by introducing a photo-acid generator to the aqueous phase which does not affect the assembly behavior of the nanoparticle surfactants, presenting a route toward adaptable interfacial assemblies. Being able to manipulate the interfacial packing of the NP surfactants using external triggers would enable a new family of materials having the desirable characteristics of fluids—rapid transport of energy carriers and controlled dissipation of mechanical energy—and the structural stability of a solid. This new class of materials can lead to revolutionary design strate-

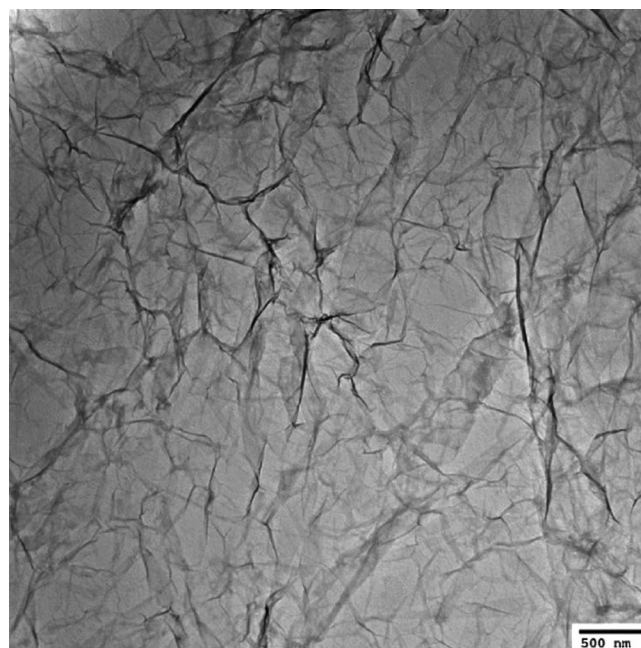


Fig. 19. TEM image of the assembled graphene film at the toluene/water interface. Reprinted with permission from Langmuir [24] © (2013) American Chemical Society.

gies for directing the flow of mechanical, electrical or optical energy in materials or system.

5 Conclusions

We have discussed the self-assembly of nanomaterials such as nanoparticles, nanorods and nanosheets at fluid interfaces. In case of fluid interfaces, the interfacial self-assembly of nanoparticles is mainly driven by the reduction of the interfacial energy. For anisotropic nanoparticles, different nanoparticle orientations can be obtained by controlling the bulk particle concentration. Self assembly of biological nanoparticles at fluid interfaces can provide a simple and fast route for the assembly of bionanoparticles into 2D or 3D constructs with hierarchical ordering. The interfacial segregation of single-walled carbon nanotubes (SWCNTs) between two immiscible liquid phases could enable applications like flexible electronic thin-film fabrication, the synthesis of porous SWCNT/polymer composites foams. The interfacial assembly of an atomically thin GO sheet at fluid interfaces opens a new route to fabricate graphene films for electronic or thin-film applications. The *in situ* formed nanoparticle surfactants due to the electrostatic interactions between the self-assembled nanoparticles and polymer at fluid interfaces would enable the generation of structured liquids. The shaped fluids represent a unique state of matter where kinetically trapped packing of NP-surfactants at interfaces leads to the kinetic trapping and shaping of liquids on the macroscopic length scale. External stimuli such as pH can be used to change the packing and properties of the NP-surfactants assemblies that, in turn, will change the shape, a macroscopic characteristic, assumed by the fluid phases.

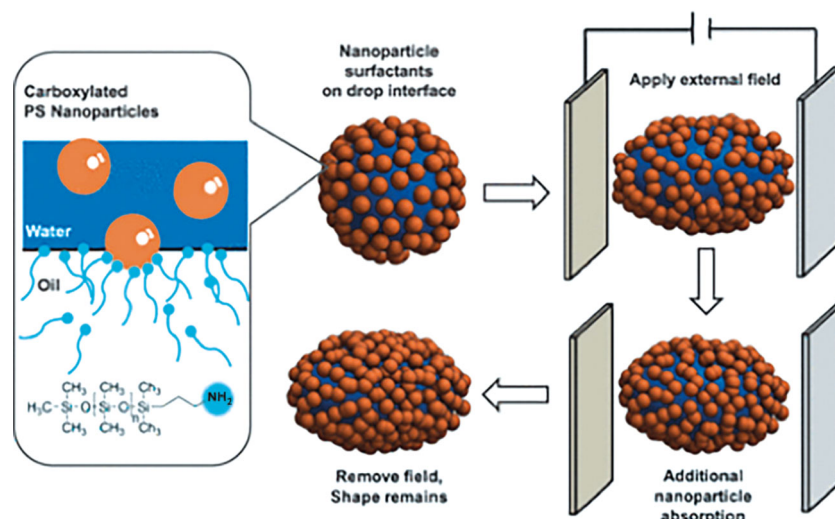


Fig. 20. Schematic representation of the deformation of a spherical drop, clad with nanoparticle surfactants, by an electric field, into an ellipsoid whose shape is maintained after the removal of the field by the interfacial jamming of the nanoparticle surfactants. Reprinted with permission from Science [25] © (2013) The American Association for the Advancement of Science.

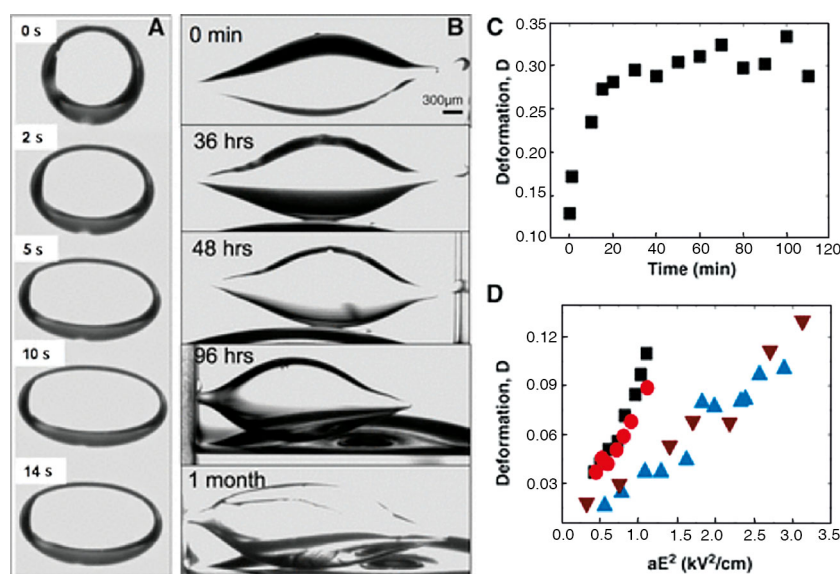


Fig. 21. The deformation and stability of drops clad with nanoparticle surfactants. (A) A time series showing the deformation of a water drop, containing 1% (by weight) dispersion of 15 nm carboxylated polystyrene nanoparticles, suspended in a silicone oil containing PDMS, end-functionalized with an amine, under a 4.6 kV/cm electric field. The diameter of the original drop is 1.8 mm. (B) A time series of a drop, clad with nanoparticle surfactants, that has been deformed in an electric field and the field has been shut off. (C) The deformation D of the water drop containing polystyrene nanoparticles in a silicone oil containing amine end-capped PDMS. D asymptotes to a well-defined value defined by the force exerted by the electric field and the reduction in interfacial energy. (D) The linear relationship between the D and aE^2 under various conditions. The maroon triangles represent pure water in pure, non-functional silicone oil; the blue triangles are results from polystyrene nanoparticles in water dispersed in a non-functional silicone oil; the red circles represent pure water in mixed silicone oils, one of which is an amine end-capped PDMS (5%); the black circles are results for a drop of an aqueous dispersion of polystyrene nanoparticles (1%) in mixed silicone oils, one of which is an amine end-capped PDMS (5%). Reprinted with permission from Science [25] © (2013) The American Association for the Advancement of Science.

6 Perspective directions

Though nanomaterial assembly at liquid-liquid interfaces yielded significant advances in both fundamental understanding and practical applications, still many areas re-

main to be explored. One is the *in situ* characterization and careful control of thin-film morphology formed at liquid-liquid interfaces, since direct microscopic observation of a transferred, dried film is prone to distortion of the true morphological information. This is of particular

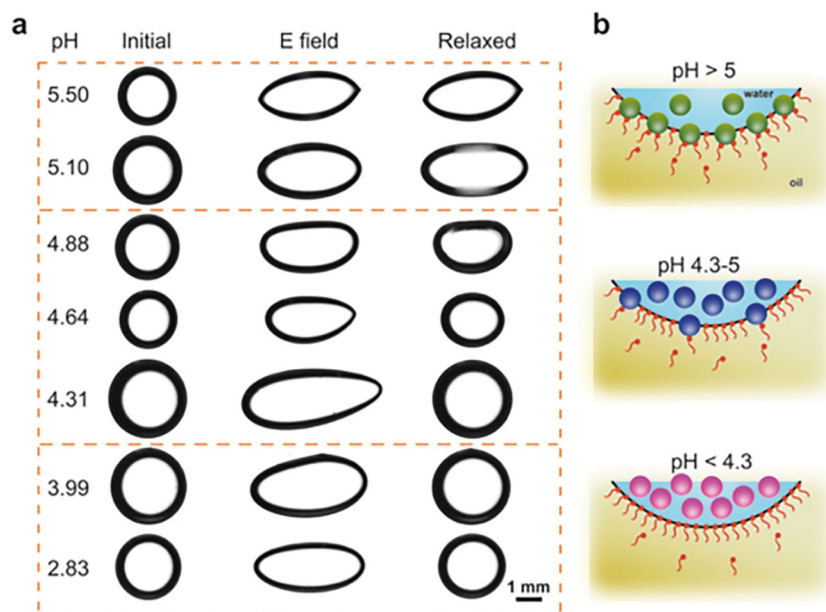


Fig. 22. Structuring and re-structuring liquids through pH controlled jamming and un-jamming of NP-surfactants. (a) The shape changing process of NP aqueous droplet (1 mg/ml) in PDMS-NH₂ silicone oil solution (10% w/w) under different pH value by applying an electric field (4.3, 3.9, 3.4, 3.0, 2.4, 1.9 and 1.5 kV/cm from top to bottom) and removing it. (b) Schematic diagram of assembly behavior between NPs and ligands under different pH value at the oil/water interfaces. Reprinted with permission [26].

importance for the manipulation of the anisotropic nanomaterials where the precise manipulation of orientation can play a big role in determining their properties. This requires a combination of scattering and microscopy techniques.

The other area that is worthwhile to investigate is the mechanical properties of the thin films. Fortunately, the cutting-edge techniques in interfacial rheology open a route to the quantitative characterization of the thin-film rheology. The comprehensive understanding of these properties provides valuable information of film dynamics and strength that are intimately related to thin-film fabrication and liquid phase stabilization, the two major applications of nanomaterials assembly at liquid-liquid interfaces.

This work was supported by the Laboratory Directed Research and Development Program of Lawrence Berkeley National Laboratory under U.S. Department of Energy Contract No. DE-AC02-05CH11231 and support through Seed Funding for a Program Seed entitled “Adaptive Interfacial Assemblies Towards Structuring Liquids” Project Number KC020301.

References

- P. Pieranski, Phys. Rev. Lett. **45**, 7 (1980).
- Y. Lin *et al.*, Langmuir **21**, 1 (2005).
- F. Reincke, S.G. Hickey, W.K. Kegel, D. Vanmaekelbergh, Angew. Chem., Int. Ed. **43**, 458 (2004).
- L. Hu, L. Wu, M. Liao, X. Fang, Adv. Mater. **23**, 1988 (2011).
- L.F. Hu, M. Chen, W.Z. Shan, T.R. Zhan, M.Y. Liao, X.S. Fang, X.H. Hu, L.M. Wu, Adv. Mater. **24**, 5872 (2012).
- H. Chen, L.F. Hu, X.S. Fang, L.M. Wu, Adv. Funct. Mater. **22**, 1229 (2012).
- W. Tian, C. Zhi, T. Zhai, X. Wang, M. Liao, S. Li, S. Chen, D. Golberg, Y. Bando, Nanoscale **4**, 6318 (2012).
- L. Hu, M. Chen, X. Fang, L. Wu, Chem. Soc. Rev. **41**, 1350 (2012).
- M. Chen, L.F. Hu, J.X. Xu, M.Y. Liao, L.M. Wu, X.S. Fang, Small **7**, 2449 (2011).
- B. Cui, H. Lin, Y.Z. Liu, J.B. Li, P. Sun, X.C. Zhao, C.J. Liu, J. Phys. Chem. C **113**, 14083 (2009).
- Y. Lin, H. Skaff, A. Boker, A.D. Dinsmore, T. Emrick, T.P. Russell, J. Am. Chem. Soc. **125**, 42 (2003).
- J. He *et al.*, Small **3**, 7 (2007).
- S. Kutuzov *et al.*, Phys. Chem. Chem. Phys. **9**, 48 (2007).
- N.F. Steinmetz, M. Manchester, *Viral Nanoparticles: Tools for Material Science and Biomedicine*, 1st edition (Pan Stanford Publishing, 2011).
- M. Uchida, S. Kang, C. Reichhardt, K. Harlen, T. Douglas, Biochim. Biophys. Acta **1800**, 8 (2010).
- J.T. Russell *et al.*, Angew. Chem. Int. Ed. **44**, 16 (2005).
- J. He *et al.*, Langmuir **25**, 9 (2009).
- S. Fujii *et al.*, Science **338**, 1 (2009).
- R. Tangirala *et al.*, Soft Matter **5**, 5 (2009).
- H. Wang, E.K. Hobbie, Langmuir **19**, 8 (2003).
- E.K. Hobbie, J.A. Fagan, J. Obrzut, S.D. Hudson, ACS Appl. Mater. Interfaces **1**, 7 (2009).
- E.K. Hobbie *et al.*, Langmuir **21**, 23 (2005).
- T. Feng, D.A. Hoagland, T.P. Russell, Langmuir **30**, 4 (2014).
- Z. Sun, T. Feng, T.P. Russell, Langmuir **29**, 44 (2013).
- M. Cui, T. Emrick, T.P. Russell, Science **342**, 6157 (2013).
- C. Huang, Z. Sun, M. Cui, F. Liu, B.A. Helms, T.P. Russell, Adv. Mater. in press.



Anju Toor received her BE degree in 2010 in Manufacturing Processes and Automation engineering from Netaji Subhas Institute of Technology, University of Delhi, India. In 2015, she received MS degree in Electrical Engineering and Computer Science at University of California Berkeley, USA. She is currently a PhD candidate in Mechanical Engineering at University of California Berkeley. Her research interests include development of nanocomposite dielectric materials, self-assembly of nanomaterials at fluid interfaces and their applications in emulsion and membrane technologies.



Tao Feng obtained his bachelors' degree in polymer materials and engineering from Beijing University of Chemical Technology in 2010. In 2016, he received his Ph.D. degree in polymer science and engineering under the joint guidance of Professor Thomas P. Russell and Professor David A. Hoagland at the University of Massachusetts at Amherst, where his research focused on the assembly and rheology of nanomaterials at liquid/liquid interfaces. He is currently a research associate at the Chinese University of Hong Kong in collaboration with the BASF chemical company to develop novel encapsulation technique.



Russell, the Silvio O. Conte Distinguished Professor of Polymer Science and Engineering at the University of Massachusetts Amherst, was a Research Staff Member at IBM Almaden Research, the Director of the Materials Research Science and Engineering Frontier Research Center on Polymer-Based Materials for Harvesting Solar Energy, is a lead PI in the WPI-Advanced Institute of Materials Research at Tohoku University, and is a PI in the Beijing Advanced Innovation Institute at BUCT. His research interests include the surface and interfacial properties of polymers, self-assembly processes, the dynamics and jamming of interfacial nanoparticle assemblies to structure fluids.